Research Article | Vol. 33, No. 8 / 21 Apr 2025 / Optics Express 18591
Optics EXPRESS

Highly sensitive double-grating interferometer for direct measurement of a neutral helium gas density in a capillary cell

KYUNGMIN ROH, YOUNGMIN LEE, HYUNIL BENJAMIN KIM, SEONGJIN JEON, HYOJEONG LEE, AND HYYONG SUK*

Department of Physics and Photon Science, Gwangju Institute of Science and Technology (GIST), Gwangju 61005, Republic of Korea
*hysuk@gist.ac.kr

Abstract: We developed a highly sensitive double-grating interferometer using four probe beams, which can measure one order of magnitude smaller phase shifts compared with other conventional interferometers. To achieve the unprecedented sensitivity, a highly dynamic 16-bit CCD camera was used and the balanced detection technique with four probe beams was employed in the 2-dimensional (2-D) interferometry for the first time. By using this interferometer, we could directly measure a low helium (He) gas density of $n \simeq 1 \times 10^{17}$ cm^{-3} in a capillary gas cell for the laser-plasma acceleration research, which is almost impossible with other conventional laser interferometers. This interferometer may provide a new tool for applications with extremely small phase shifts in science.

1. Introduction

Laser interferometry is a very powerful technique that is widely used in diverse areas. One of the important applications is plasma diagnostics, where the plasma density can be measured using the phase shift caused by the optical path difference in the plasma. In fact, several types of laser interferometers are often used for plasma diagnostics. For example, the Michelson interferometer [1], the Mach-Zehnder interferometer [2], and the Nomarski interferometer [3] have been utilized so far for plasma density diagnostics in the laser-plasma acceleration research. However, those conventional laser interferometers have a limitation in the measurement of very small phase shifts.

In the laser plasma acceleration research for high energy electron generation [4], helium (He) gas jets [5,6] and gas cells/capillary gas cells [7–9] are widely used as a plasma source up to now and their plasma densities are generally on the order of 10^{18} cm^{-3}. This plasma density range can be easily measured using conventional interferometers, as the refractive index difference between plasma and vacuum is greater than that between gas and vacuum. In order to obtain higher electron energies in the laser-plasma acceleration, however, the plasma density should be decreased down to the level of 10^{17} cm^{-3} [10], leading to a much smaller phase shift in the interferogram. In this density range, however, the neutral helium gas has two orders of magnitude smaller phase shift compared with the plasma. That is why the direct measurement of a helium gas density using the transverse interferometry in a capillary gas cell has not been reported so far although the plasma density down to $n_e \simeq 10^{17}$ cm^{-3} was measured in the discharge capillary waveguide [2]. It implies that the direct measurement of helium gas density is extremely difficult. Hence, conventional interferometers are not able to provide the gas density information directly, for example, in capillary gas cells with only a few hundred μm hole size in the transverse direction. However, it will be more advantageous if we can measure the neutral He gas density directly, compared with the density measurement of the laser-produced plasma. This is because the capillary structure with a tiny hole can be easily damaged by the focused high-power (>TW) laser

#562060 https://doi.org/10.1364/OE.562060
Journal © 2025 Received 12 Mar 2025; revised 6 Apr 2025; accepted 7 Apr 2025; published 18 Apr 2025

Optics EXPRESS

pulse for high energy electron generation in the capillary gas cell. In addition, efforts to have an indirect measurement of the neutral gas density from plasma diagnostics [11,12] inherently require plasma generation, which causes the surface erosion and damage on the transparent capillary material, for example, sapphire, leading to fundamental limitations on their applicability for measurement of the longitudinal density profile. Therefore, it will be more beneficial if one can measure the neutral He gas density and spatial density profile inside the capillary cell before sending high power laser pulses into the capillary hole for experiments. That is why we developed a novel interferometer with much higher sensitivity.

In this paper, we introduce our novel approach to significantly enhance the sensitivity of interferometric measurements, making it possible to measure the low gas density of He with unprecedented precision. This enhanced detection method incorporates three key advancements. First, a novel concept of an interferometer based on double gratings (see our previous relevant work in Ref. [13]) is utilized, which is highly resistant to mechanical vibrations. Second, the balanced detection technique is employed in 2-D interferometery for the first time, leading to doubling the signal-to-noise ratio (SNR). For this purpose, we used four probe beams instead of two beams which are common in conventional interferometers. Third, the measurement sensitivity is further improved by employing a 16-bit CCD camera with a highly dynamic range, compared with commonly used 12-bit cameras. As a result of those features, the enhanced interferometer was successfully demonstrated to provide much lower He gas density information in a capillary gas cell, which is almost impossible with other conventional interferometers. In the case of gas jets, helium gas density measurements of the order of 1×10^{18} cm^{-3} were reported [14]. In our experiment, however, the lowest measured helium gas density inside the capillary gas cell reached down to the level of 1×10^{17} cm^{-3}. To the best of our knowledge, this is the first report of a direct measurement of the helium density map in that range. Details of the development and application of the highly sensitive interferometer are described in the following sections.

2. Development of a highly sensitive interferometer

2.1. Novel concept of a double-grating interferometer using four beams

A novel interferometer concept was developed for the application of the balanced detection technique to capillary gas cell diagnostics, based on the double-grating differential interferometer we previously reported [13]. The main difference from the previous work is that its optical scheme employs *four* probe beams instead of *two* beams used in the previous case. We used this kind of special design to apply the balanced detection technique for capillary gas cell diagnostics, which was not possible with the previous configuration or any other conventional interferometers that use only two beams. Furthermore, this interferometer belongs to the category of common-path interferometers such as the Nomarski interferometer, which offers greater stability against environmental noise sources, including mechanical vibrations and temperature changes [15]. Unlike gas jets, capillary gas cells have rather large structures, requiring a long shear distance to obtain a reference beam that does not pass through the capillary gas cell. In other shearing interferometers like the Nomarski interferometer, this long shear distance prevents capturing two separate images of the capillary gas cell within a single frame, which is necessary for balanced detection in our case. The double-grating interferometer is particularly important in this experiment because it enables the simultaneous use of multiple diffraction orders, producing two images with opposite phase signs. By using the double-grating interferometer, four images can be used to form interference patterns, and among them, two images with opposite phases can be brought close together as shown in Fig. 1(b). Those two images with opposite phase signs are captured by a single CCD camera, and they can be used for balanced detection.

The double-grating interferometer employs two identical gratings with repeated light-blocking patterns, and its optical configuration is shown in Fig. 1(a). In this scheme, the first grating G_1 and

Optics EXPRESS

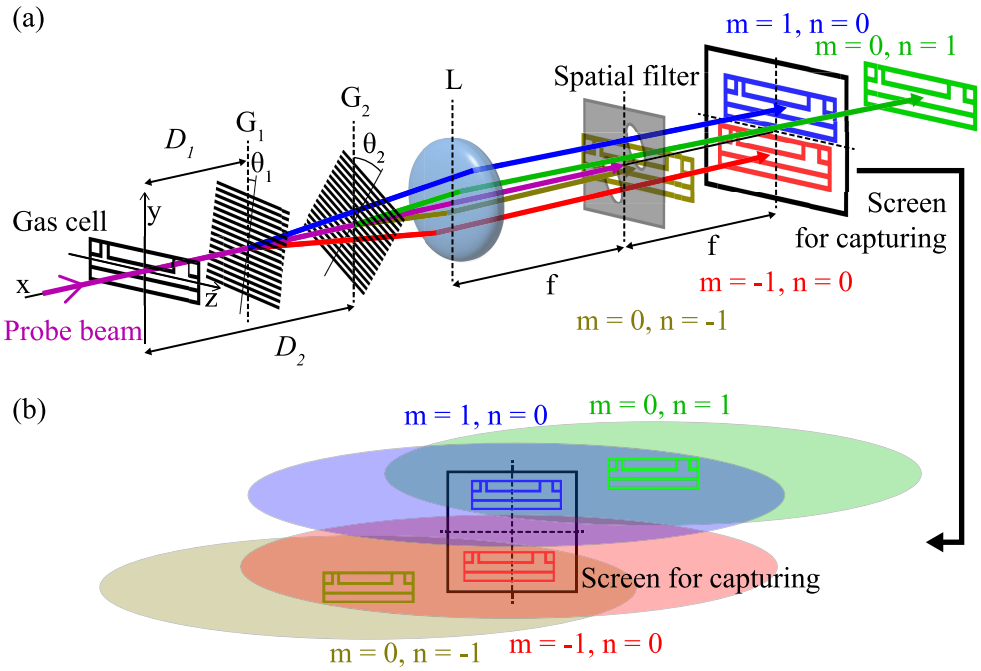

Fig. 1. (a) Schematic of the double-grating differential interferometer for four beam imaging. G_1 and G_2: gratings, D_1 and D_2: distances between the capillary gas cell and each grating, L: an imaging lens, f: focal length of the imaging lens. Four first-order diffracted beams are designed to pass through the spatial filter positioned at the focal plane of the lens L, while the zero order beam is blocked by the spatial filter. The transmitted four beams form two separate interferograms with opposite phase signs that are close to each other, and the two interferograms of $m = \pm 1$ are captured by a single CCD camera. The details on the screen are shown in (b).

the second grating G_2 are positioned at distances D_1 and D_2 from the gas cell, respectively, and they are tilted at angles θ_1 and θ_2 relative to the y-axis. Four diffraction orders [$(m = +1, n = 0)$, $(m = 0, n = +1)$, $(m = -1, n = 0)$ and $(m = 0, n = -1)$] are selected by the spatial filter in the focal plane of the imaging lens, satisfying the diffraction order conditions $m + n = +1$ (positive first-order) and $m + n = -1$ (negative first-order), where m and n represent the diffraction orders of the first and second gratings, respectively. The intensity distribution in the gas cell object plane, which is imaged onto the CCD camera, is deformed by the two gratings. The result can be obtained by using the scalar diffraction theory [13]. The intensity distributions of the positive first-order diffracted beam I_{+1} and the negative first-order diffracted beam I_{-1} are calculated as follows:

$$I_{+1}(y,z) \propto 1 + \cos\left[\frac{2\pi(\cos\theta_1 - \cos\theta_2)}{d}y - \frac{2\pi(\sin\theta_1 - \sin\theta_2)}{d}z + \frac{k(D_1 - D_2)\lambda^2}{2d^2} + \Delta\varphi\left(y - \frac{D_1\lambda\cos\theta_1}{d}, z - \frac{D_1\lambda\sin\theta_1}{d}\right) - \Delta\varphi\left(y - \frac{D_2\lambda\cos\theta_2}{d}, z - \frac{D_2\lambda\sin\theta_2}{d}\right)\right], \tag{1}$$

$$I_{-1}(y,z) \propto 1 + \cos\left[\frac{2\pi(\cos\theta_2 - \cos\theta_1)}{d}y - \frac{2\pi(\sin\theta_2 - \sin\theta_1)}{d}z - \frac{k(D_2 - D_1)\lambda^2}{2d^2} - \Delta\varphi\left(y + \frac{D_1\lambda\cos\theta_1}{d}, z + \frac{D_1\lambda\sin\theta_1}{d}\right) + \Delta\varphi\left(y + \frac{D_2\lambda\cos\theta_2}{d}, z + \frac{D_2\lambda\sin\theta_2}{d}\right)\right], \tag{2}$$

Optics EXPRESS

where d is the grating period, λ is the wavelength of the probe beam, and $k = 2\pi/\lambda$ is the wave number. In these equations, the two positive first-order diffracted beams [$(m = +1, n = 0)$ and $(m = 0, n = +1)$] shear to the $+y$ and $+z$ directions, while the two negative first-order diffracted beams [$(m = -1, n = 0)$ and $(m = 0, n = -1)$] shear to the $-y$ and $-z$ directions. The shear distance induced by the first grating and the second grating are $D_1\lambda/d$ and $D_2\lambda/d$, respectively. Now it is evident why four beams are used in our interferometer. To form an interference pattern with a reference beam that does not pass through the capillary gas cell, a long shear distance is required. In conventional interferometers using only two beams, this large shear distance makes it difficult to capture both images within a single frame. In our double-grating interferometer, the distance between the two capillary images of $m + n = 1$ or $m + n = -1$ must be sufficiently larger than the size of the capillary structure to obtain non-overlapping images. This can be achieved by setting the angle θ_2 to a relatively large value (e.g., $\theta_2 \approx 45°$) and appropriately adjusting the distance D_2. Furthermore, the two images diffracted by the first grating should be close enough, so they can be captured by the single CCD camera. This can be achieved by setting the angle θ_1 to a small value (e.g., $\theta_1 \approx 0°$) and appropriately adjusting the distance D_1. The grating period d is not as critical as the other parameters since the shear distance can be adjusted by changing the distances D_1 and D_2. As shown in Fig. 1, the two diffracted beams [$(m = 1, n = 0)$ and $(m = -1, n = 0)$] are formed closely with a separation distance $2D_1\lambda/d$ and the other two diffracted beams [$(m = 0, n = 1)$ and $(m = 0, n = -1)$] provide reference beams to generate interference patterns. Additionally, the phase shifts in these two images [$(m = 1, n = 0)$ and $(m = -1, n = 0)$] have opposite signs as shown in Eqs. (1) and (2), so we can use the balanced detection technique, leading to a higher SNR signal.

Typical interferograms from the double-grating interferometer are shown in Fig. 2. In this figure, two images of the capillary gas cell are shown sheared almost in the vertical direction, which is due to the small angle θ_1. It should be noted that the phase shifts by gas in two gas cell images have opposite signs. For example, if the fringes in the red line are shifted in the right direction, fringes in the blue line will be shifted in the left direction. The area below the capillary hole structure is used to obtain a reference phase shift, which helps elimination of the phase shifts not induced by the gas, for instance, those caused by mechanical movements due to gas injection.

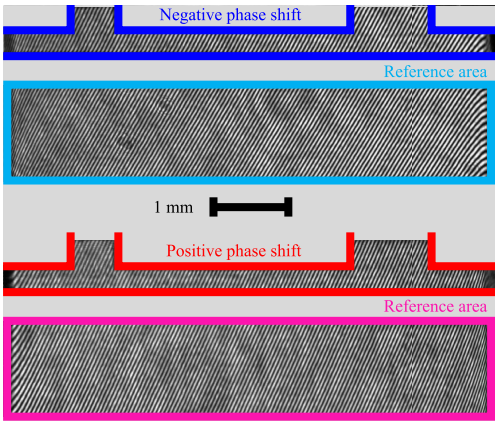

Fig. 2. Typical interferograms of the gas-filled capillary cell from the double-grating interferometer. The red and blue lines indicate the two identical gas cell images with opposite signs in phase shift. They are captured within a single frame by obtaining the reference beam from outside the gas cell, where large shear distances are required to form the interference fringes.

Optics EXPRESS

2.2. Balanced detection in 2-D interferometry for doubling the signal amplitude

Balanced detection is a well-known technique in optoelectronics, which can effectively enhance the signal-to-noise ratio. This technique uses two identical signals with opposite signs. When these signals are subtracted, common noises in both signals are canceled out, and the resulting signal amplitude is doubled. Balanced detection has been widely applied in one-dimensional (1-D) interferometry using two balanced photodetectors [16,17]. However, this technique has not been implemented in 2-D imaging interferometry as far as we know. In our work, the application of balanced detection in 2-D interferometry is made possible by using the double-grating shearing interferometer. In the obtained interferograms in our case, the two images have opposite phase signs with the same amplitude and the phase shift amplitude can be doubled by subtracting the two phase shifts, while common noises are effectively canceled. This method can significantly improve the measurement sensitivity and precision in our 2-D interferometry. In Fig. 3, for example, three phase shifts from the helium-filled capillary gas cell with a backing pressure of 300 mbar are compared to demonstrate the effectiveness of the balanced detection. In Fig. 3(a), the images of positive and negative phase shifts are shown, which are obtained from the regions enclosed by the red and blue lines in Fig. 2, respectively. Subsequently, the phase shifts with opposite signs are subtracted from each other, and as a result, a signal with a doubled amplitude can be obtained, as shown in Figs. 3(a) and 3(b).

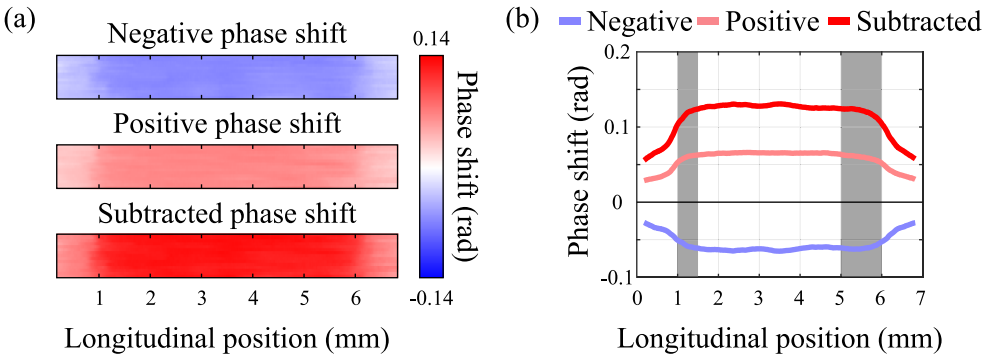

Fig. 3. (a) 30-shot-averaged example phase shift maps with 300 mbar helium gas in the capillary cell. The negative phase shift (top) and the positive phase shift (middle) are subtracted for balanced detection (bottom). (b) The longitudinal line profiles of the negative phase shift (blue), the positive phase shift (pink) and the subtracted phase shift (red). The gray-shaded areas indicate the locations of the two gas injection feedlines in the capillary cell, of which the detailed structure will be given in the next section.

2.3. Higher dynamic range detection for increased sensitivity

Using a high-dynamic-range 16-bit camera can significantly enhance the sensitivity of the interferometer. This is because the sensitivity of 2-D interferometric measurements is directly related not only to the spatial resolution of the camera capturing the interference patterns but also to the intensity resolution of its pixels. A higher spatial resolution of the camera results in greater measurement accuracy since the phase shift in the interference patterns is determined by measuring the fringe shift. Additionally, as the fringes shift, the intensity at fixed positions in the images varies. Accurate measurement of these intensity variations is also a crucial factor for determining the phase shift. Therefore, a higher bit depth, which corresponds to the higher intensity resolution, allows more precise measurements [18]. This effect was tested using three cameras with different dynamic ranges (8-bit, 12-bit, and 16-bit) as shown in Fig. 4. To ensure that the result is influenced only by the camera's dynamic range, interferograms without the gas

Optics EXPRESS

cell were acquired under the same conditions. For each camera, 30 signal-free interferograms were captured with a 1-second exposure time and the same fringe width. The phase shifts were extracted using the 1-D wavelet transform [19] and their standard deviations were compared. The results indicate that the 16-bit camera gives a much higher dynamic range in the signal compared with others, of course, as shown in Fig. 4(a). Furthermore, Fig. 4(b) shows that the 16-bit CCD camera provides the lowest standard deviation, demonstrating that the sensitivity of the interferometer is significantly affected by the dynamic range of the camera. This effect becomes particularly significant when the phase shifts to be measured are very small. The estimated phase shift in our capillary gas cell filled with helium at an atomic density of 2.3×10^{18} cm^{-3} is approximately 20 mrad, which corresponds to a fringe shift of 0.16 pixels assuming one fringe period is 50 pixels. In such cases, it is necessary to measure the intensity variations at each pixel instead of measuring the phase shift by tracking the fringe movement. Therefore, the bit depth of the camera plays a crucial role in sensitivity. For a phase shift of 20 mrad, the maximum intensity variation is estimated to be 650 if the full dynamic range of a 16-bit camera is used. This fact suggests that, by employing a 16-bit camera with minimized noises, it is possible to accurately measure small phase shifts in the interferogram induced by low-density helium gas.

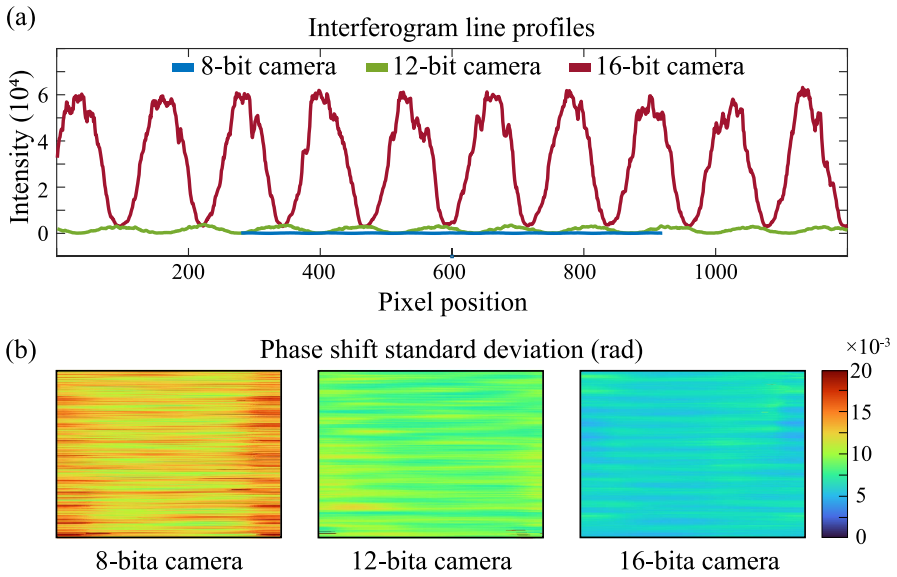

Fig. 4. (a) Comparison of line intensity profiles of the interference patterns captured by the 8-bit (blue), 12-bit (green) and 16-bit (red) cameras, and (b) their standard deviation maps of the phase shift in each case. This result shows that the standard deviation in phase shift is significantly smaller in the 16-bit CCD camera compared with others.

3. Experiments for diagnostics of the low density He gas in the capillary cell

3.1. Experimental setup

By using the developed interferometer, we performed experiments to measure the He gas density directly in a capillary cell for laser-plasma acceleration. An optical scheme of the highly sensitive interferometry system is shown in Fig. 5(a). In this experimental setup, a continuous-wave diode laser (MDL-III-405, CNI) with a wavelength of 405 nm and an output power of 100 mW was spatially filtered using an 8 μm pinhole to make a uniformly distributed beam profile, and then it was sent to the gas-filled capillary as a probe beam for interferometry. Here, it should be noted that the probe beam is expanded to a large beam so that it can cover the entire capillary size. In

Optics EXPRESS

this experiment, the previously developed capillary gas cell [8] was used. After the probe beam traverses the capillary gas cell across the capillary hole, an image is formed using the telescope with two plano-convex lenses (f = 300 mm) and the image plane is imaged again using a bi-convex lens (f = 300 mm) onto the cooled 16-bit CCD camera (MLx285, FLI). A specially designed double-grating interferometer was employed to obtain the phase shift information induced by the gas filled in the capillary cell. The double-grating interferometer consists of two Ronchi gratings (30 lp/mm): one positioned close to the image plane, while the other was placed far from it.

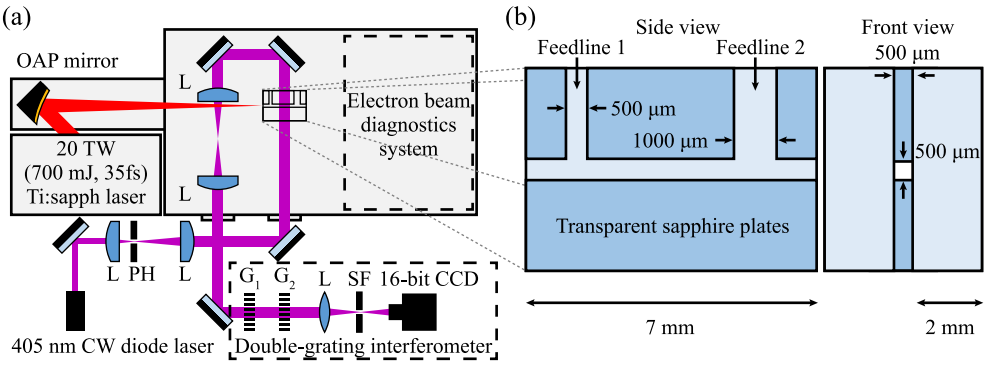

Fig. 5. (a) Schematic diagram of the experimental setup for He gas diagnostics in the capillary cell. L: lens, PH: pinhole, G: grating, SF: spatial filter, OAP mirror: off-axis parabolic mirror. (b) Detailed structure of the capillary gas cell consisting of four polished sapphire plates. The capillary structure is transparent and features a rectangular cross-section for interferometric measurements. Different backing pressures can be applied to the first and second gas feedlines, respectively, through separate gas injection lines.

The capillary gas cell consists of four sapphire plates with polished surfaces that are optically transparent, enabling interferometric measurements, as shown in Fig. 5(b). Two 500 μm thick sapphire plates are positioned with a spacing of approximately 500 μm between two 2-mm thick sapphire plates to form the capillary structure. One of the two thin sapphire plates with 500 μm in thickness was machined to have two gas feedlines with widths of 500 μm and 1000 μm respectively. The two gas feedlines are independently connected to separate gas lines, allowing different backing pressures to each feedline. All sapphire plates are fastened by a holding structure connected to two high-speed solenoid valves (Parker Hannifin, model 009-0181-900). Helium gas was filled in the capillary cell through the two gas injection feedlines by opening the pulsed gas valves.

3.2. *Longitudinal He gas density distribution in the capillary gas cell*

In laser-plasma acceleration experiments for high energy electron generation, a high power laser pulse should be focused into the small hole of the capillary gas cell and the laser pulse should pass through the capillary hole, as shown in Fig. 5. In this process, the gas density along the axial capillary hole is very important as it will severely affect the generated electron beam energy. Therefore, the longitudinal gas density profile inside the capillary cell must be investigated thoroughly before electron acceleration experiments with high-power laser pulses.

To study the longitudinal gas density distribution, the 405 nm probe beam was transmitted transversely through the capillary gas cell hole, as shown in Fig. 5(a). Before capturing the interferogram images with phase shifts induced by the He gas, a reference interferogram was recorded without gas injection for every shot with 1-second exposure time. After acquiring the reference images, the two gas valves were opened for 100 ms to reach the steady state, and then the signal interferograms were captured, also with a 1-second exposure time. According to our

Optics EXPRESS

previous research [8], the filling time of the gas cell is approximately 60 ms, indicating that a steady-state condition is reached after this time duration. Once the interferograms were obtained, their phase shifts were analyzed using the 1-D wavelet transform. The measured phase shifts were used to calculate the gas density inside the capillary gas cell. The relation between phase shift $\Delta\varphi$ and refractive index n is given by $\Delta\varphi = 2\pi\,(n-1)\,L/\lambda$, where λ is the wavelength of the probe beam and L is the length of the medium which is the transverse size of the capillary hole in our case. The Lorentz–Lorenz equation [20] was used for the calculation of the molecular gas density N. As a result, the molecular gas density can be derived from the measured phase shift using the equation given by $N = (\lambda\Delta\varphi)/(4\pi^2\alpha L)$, where α is the polarizability of the gas molecule. The polarizability α can be directly calculated from the refractive index with known temperature, pressure and wavelength using the equation given by $\alpha = [RT(n-1)]/(2\pi P N_A)$, where $R = 8.314\ \mathrm{J\cdot K^{-1}\cdot mol^{-1}}$ is the ideal gas constant, T is the temperature (K), P is the pressure (Pa) and $N_A = 6.022 \times 10^{23}\ \mathrm{mol^{-1}}$ is the Avogadro constant. The calculated polarizability is $\alpha = 0.208 \times 10^{-24}\ \mathrm{cm^3}$ for the helium gas from the refractive index of 1.0000346 with 1 bar and 273 K for 405 nm wavelength. Using the calculated polarizability, the gas density map was obtained from the retrieved phase shift map.

The capillary gas cell was filled with helium gas using the first feedline (500 μm) and the second feedline (1000 μm), both operated at the same backing pressure. Then, the molecular helium gas densities were obtained with different backing pressures ranging from 0 to 500 mbar. The result is shown in Fig. 6(a), where higher densities can be obtained for higher backing pressures. Furthermore, it is shown that the longitudinal density profile inside the capillary gas cell is quite uniform. This is a very important feature compared with gas jets which have nonuniform density profiles in general. Furthermore, since the two gas feedlines are connected to separate gas lines, different gas pressures can be applied to each gas line to form tapered gas density profiles inside the capillary gas cell, which is intended to extend the dephasing length for generation of higher electron beam energies [21,22]. The longitudinal density gradient in the capillary can be controlled by adjusting the ratio between the two gas injection backing pressures. This effect was clearly observed in our experiments, as shown in Fig. 6(b). The helium gas densities were measured by keeping the backing pressure in the first feedline fixed at 100 mbar and varying the backing pressure in the second feedline from 100 to 300 mbar. The result shows that tapered gas densities can be produced and the density gradient along the longitudinal direction can be controlled, as shown in Fig. 6(b). This is an excellent feature of our capillary gas cell for laser-plasma acceleration research.

In order to test the limitation of this interferometer, we diagnosed the helium density inside the capillary gas cell at the lowest backing pressure that can be applied to the feedlines, which is about 33 mbar in our gas valve system. To improve the measurement accuracy, the exposure time for interferometry was increased from 1 second to 5 seconds, and then 30 measurements were taken and averaged. As shown in Fig. 7, the helium gas density between the two feedlines with an injection pressure of 33 mbar is around $6\times10^{17}\ \mathrm{cm^{-3}}$ and it drops sharply near the capillary hole exits. This fact implies that the double-grating interferometer can be used for lower helium gas densities. Finally, we closed both valves in the gas system to evaluate the noise level of the measurements, and the result is shown in the orange color in Fig. 7. For this purpose, the 30-shot averaged longitudinal helium density was used for the standard deviation calculation and it gave a noise level of $\simeq 1\times10^{17}\ \mathrm{cm^{-3}}$. Tens of measurements of the longitudinal density profile revealed that the result of Fig. 7 was repeatable although the density profile fluctuated within the standard deviation.

The most critical issue in this experiment is the random environmental noise. Since our double-grating interferometer was designed as an in-situ diagnostic tool for high-power laser experiments, it is inevitably exposed to a noisy environment, including thermal drift, air fluctuation, mechanical movement, and laser source instability. These types of noise were suppressed using methods

Optics EXPRESS

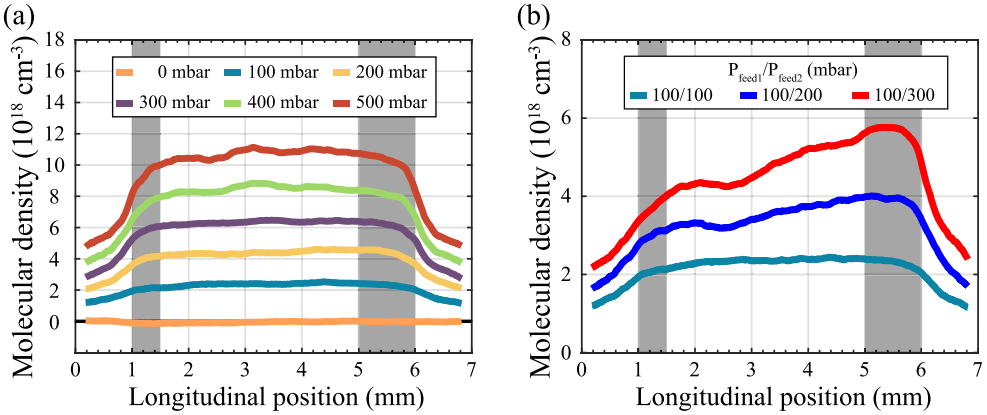

Fig. 6. (a) Helium gas density profiles inside the capillary gas cell at backing pressures from 0 to 500 mbar. The shaded gray areas indicate two gas feedlines with 500 μm and 1000 μm in width, respectively. Here, the same gas pressure was applied to the two gas feedlines. (b) Tapered helium density profiles by increasing the pressure in the second gas feedline, which implies that the density slope can be controlled in the capillary gas cell.

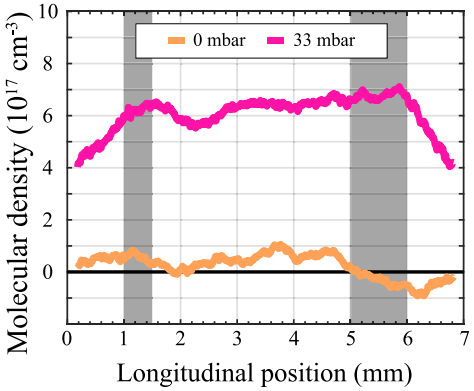

Fig. 7. Helium gas density profiles at a backing pressure of 33 mbar (magenta), which is the lowest achievable backing pressure in our gas system, and at a backing pressure of 0 mbar (orange) in both of the gas valves.

such as reference subtraction, balanced detection, and averaging. However, these methods resulted in the long measurement duration of 5 seconds. This limitation could be solved by introducing additional techniques. For instance, application of the multi-pass probing to our interferometer will increase the signal amplitude, thereby enhancing the SNR, which implies that the measurement time can be reduced.

4. Conclusions

It was demonstrated that the sensitivity of interferometry can be significantly enhanced by our proposed method, which employs the four-beam-based double-grating interferometer with the 2-D balanced detection technique and a highly dynamic CCD camera. The developed interferometer showed that a low helium gas density down to $n \simeq 1 \times 10^{17}$ cm^{-3} can be directly diagnosed in a capillary gas cell, which is impossible by other conventional interferometers. In addition, our interferometer has the potential to enhance the sensitivity further by employing the multi-pass

Optics EXPRESS

probing technique. The highly sensitive 2-D interferometry proposed in this paper may be useful for many other areas where conventional interferometers cannot be used due to too small phase shifts.

Funding. National Research Foundation of Korea (RS-2022-NR070637, RS-2023-00218180, RS-2022-00154676).

Disclosures. The authors declare no conflicts of interest.

Data availability. The raw data of this paper are not publicly available at this time but may be obtained from the authors upon reasonable request.

References

1. R. E. Walkup, J. M. Jasinski, and R. W. Dreyfus, "Studies of excimer laser ablation of solids using a Michelson interferometer," Appl. Phys. Lett. **48**(24), 1690–1692 (1986).
2. A. J. Gonsalves, T. P. Rowlands-Rees, B. H. P. Broks, *et al.*, "Transverse interferometry of a hydrogen-filled capillary discharge waveguide," Phys. Rev. Lett. **98**(2), 025002 (2007).
3. R. Benattar, C. Popovics, and R. Sigel, "Polarized light interferometer for laser fusion studies," Rev. Sci. Instrum. **50**(12), 1583–1586 (2008).
4. T. Tajima and J. M. Dawson, "Laser electron accelerator," Phys. Rev. Lett. **43**(4), 267–270 (1979).
5. K. Schmid and L. Veisz, "Supersonic gas jets for laser-plasma experiments," Rev. Sci. Instrum. **83**(5), 053304 (2012).
6. S. Lorenz, G. Grittani, E. Chacon-Golcher, *et al.*, "Characterization of supersonic and subsonic gas targets for laser wakefield electron acceleration experiments," Matter Radiat. Extremes **4**(1), 015401 (2019).
7. J. Osterhoff, A. Popp, Z. Major, *et al.*, "Generation of stable, low-divergence electron beams by laser-wakefield acceleration in a steady-state-flow gas cell," Phys. Rev. Lett. **101**(8), 085002 (2008).
8. J. Kim, V. L. J. Phung, K. Roh, *et al.*, "Development of a density-tapered capillary gas cell for laser wakefield acceleration," Rev. Sci. Instrum. **92**(2), 023511 (2021).
9. C. Aniculaesei, H. T. Kim, B. J. Yoo, *et al.*, "Novel gas target for laser wakefield accelerators," Rev. Sci. Instrum. **89**(2), 025110 (2018).
10. A. J. Gonsalves, K. Nakamura, J. Daniels, *et al.*, "Petawatt laser guiding and electron beam acceleration to 8 gev in a laser-heated capillary discharge waveguide," Phys. Rev. Lett. **122**(8), 084801 (2019).
11. D. G. Jang, M. S. Kim, I. H. Nam, *et al.*, "Density evolution measurement of hydrogen plasma in capillary discharge by spectroscopy and interferometry methods," Appl. Phys. Lett. **99**(14), 141502 (2011).
12. D. J. Spence and S. M. Hooker, "Investigation of a hydrogen plasma waveguide," Phys. Rev. E **63**(1), 015401 (2000).
13. K. Roh, H. Lee, S. Jeon, *et al.*, "Development of a double-grating differential interferometer for plasma diagnostics," Opt. Express **32**(6), 9800–9808 (2024).
14. S. Karatodorov, R. Lera, M. Raclavsky, *et al.*, "Multi-pass probing for high-sensitivity tomographic interferometry," Sci. Rep. **11**(1), 15072 (2021).
15. Q. Liu, M. Ma, X. Zhang, *et al.*, "Application of Nomarski interference system in supersonic gas-jet target diagnosis," AIP Adv. **11**(1), 015145 (2021).
16. D. L. Mazzoni and C. C. Davis, "Trace detection of hydrazines by optical homodyne interferometry," Appl. Opt. **30**(7), 756–764 (1991).
17. J. P. Waclawek, C. Kristament, H. Moser, *et al.*, "Balanced-detection interferometric cavity-assisted photothermal spectroscopy," Opt. Express **27**(9), 12183–12195 (2019).
18. O. A. Skydan, F. Lilley, M. J. Lalor, *et al.*, "Quantization error of ccd cameras and their influence on phase calculation in fringe pattern analysis," Appl. Opt. **42**(26), 5302–5307 (2003).
19. J. Zhong and J. Weng, "Phase retrieval of optical fringe patterns from the ridge of a wavelet transform," Opt. Lett. **30**(19), 2560–2562 (2005).
20. H. A. Lorentz, "Ueber die beziehung zwischen der fortpflanzungsgeschwindigkeit des lichtes und der körperdichte," Ann. Phys. **245**(4), 641–665 (1880).
21. P. Sprangle, J. R. Peñano, B. Hafizi, *et al.*, "GeV acceleration in tapered plasma channels," Phys. Plasmas **9**(5), 2364–2370 (2002).
22. H. Suk, C. Kim, G. Kim, *et al.*, "Energy enhancement in the self-injected laser wakefield acceleration using tapered plasma densities," Phys. Lett. A **316**(3-4), 233–237 (2003).